Pion absorption above the Δ(1232) resonance

M. K. Jones,* R. D. Ransome, V. R. Cupps,† and R. W. Fergerson‡
Rutgers University, Piscataway, New Jersey 08855

C. L. Morris and J. A. McGill§
Los Alamos National Laboratory, Los Alamos, New Mexico 87545

J. D. Zumbro**
University of Pennsylvania, Philadelphia, Pennsylvania 19104
and Los Alamos National Laboratory, Los Alamos, New Mexico 87545

J. R. Comfort, B. G. Ritchie, and J. R. Tinsley††
Arizona State University, Tempe, Arizona 85287

P. C. Gugelot
University of Virginia, Charlottesville, Virginia 22901

C. Fred Moore
University of Texas at Austin, Austin, Texas 78712
(Received 18 February 1992; revised manuscript received 13 August 1993)

Two-proton and three-proton inclusive π^+ absorption cross sections were measured for incident pion energies from 250 to 500 MeV on targets of ^{12}C, ^{58}Ni, ^{90}Zr, ^{118}Sn, and ^{208}Pb using a large solid angle bismuth germanate detector array. Pion absorption events leading to three or more protons in the final state were observed to become more significant with increasing incident pion energy and were dominant at 500 MeV. The total absorption cross sections were inferred from analyses of the data with uncertainties of approximately 25%.

PACS number(s): 25.80.Ls

I. INTRODUCTION

While the experimental information on pion interactions well above the Δ(1232) resonance is rather limited, pion absorption has been observed to be a significant fraction of the pion-nucleus reaction cross section for all energies measured up to 300 MeV [1]. The pion absorption cross section on deuterium decreases from a peak of 12 mb near 140 MeV to about 0.5 mb by 500 MeV. Similarly, in ^{3}He pion absorption cross sections show a marked decrease as the pion energy increases. The absorption cross section for heavier nuclei, however, does not appear to decrease as dramatically as for deuterium for pion energies between 150 and 300 MeV. The energy dependences of the absorption cross sections for energies above 315 MeV for heavy nuclei are unknown.

Early models of pion absorption emphasized quasideuteron absorption (QDA) as the dominant mechanism for pion absorption in nuclei, particularly near the resonance [2]. However, several experiments at energies both below and above resonance have given indications that the process is more complicated and involves an increasing fraction of three-nucleon absorption at higher incident pion energies. The interpretation of the data is complicated by the presence of initial and final state interactions (ISI/FSI), which can be substantial, especially in heavy nuclei.

Kinematically complete measurements of pion absorption on ^{3}He and ^{4}He, in which ISI/FSI are expected to be less important and corrections for them more easily made, offer the clearest evidence for three-nucleon absorption processes near resonance [3–11]. A study of the $^3\mathrm{He}(\pi^+, 3p)$ reaction at $T_\pi = 350$ and 500 MeV showed that 45% of the absorption cross section was due to a three-nucleon mechanism, significantly larger than the $25 \pm 10\%$ found near the Δ(1232) resonance [12]. Calculations by Oset *et al.* [13] predict that the three-nucleon processes should be about 55% of the total absorption cross section for incident pion energies between 250 to 350 MeV, in approximate agreement with the data. However, other approaches, such as that of Masutani and

* Present address: College of William and Mary, Department of Physics, Williamsburg, VA 23187.
† Present address: Fermi National Laboratory, Batavia, IL 60510.
‡ Present address: Centigram Communications Corp., 91 East Tasman Drive, San Jose, CA 95134.
§ Present address: SSC, 2550 Beckleymeade Ave., Dallas, TX 75237.
** Permanent address: Los Alamos National Laboratory, Los Alamos, NM 87545.
†† Present address: EG&G/EM, 130 Robin Hill Rd., Goleta, CA 93116.

Yazaki [14], do not explicitly include three-nucleon processes and also give a reasonable description of the data. Another mechanism involving four nucleons, the double-Δ(1232) mechanism, has been proposed by Brown *et al.* [15]. This would be expected to increase in importance as the pion energy increased, but its relative strength to other mechanisms is unknown. Measurements on heavier nuclei are more difficult to interpret than those on light nuclei, but studies of both the $^{12}C(\pi^+, 3p)$ reaction [16, 17] and the $^{6}Li(\pi^+, 2p)$ and $(\pi^+, 3p)$ reactions [18] also gave evidence for three-nucleon processes near resonance.

Pion absorption differs from many experiments in that the signal is the absence of a particle. In principle, the measurement can be done by using a 100% efficient 4π detector and rejecting all events in which a pion is present, or by finding that the total kinetic energy of outgoing particles is greater than the incident pion kinetic energy minus the binding energy of the particles. In practice, detectors cover less than the full solid angle and do not have 100% detection efficiency for all particles at all energies. Determination of the total absorption cross section requires correcting for events containing an unobserved pion in the final state, a procedure which cannot, in general, be done unambiguously.

In the experiment described here, we use a large solid angle detector with good efficiency for charged particle detection. This allows the rejection of a substantial fraction of the events with a pion in the final state, and is combined with a study of the summed proton energy spectra to determine the π^+ absorption cross section. Pion energies up to 500 MeV were used in order to provide the first such measurement on nuclei heavier than ^{4}He for pion energies well above the Δ(1232) resonance.

II. EXPERIMENT

A. Pion beam and targets

The experiment was performed at the Pion Particle Physics channel (P^3) of the Clinton P. Anderson Meson Physics Facility (LAMPF). Positive pions with energies of 250, 300, 400, and 500 MeV were used. The pion beam was defined by a 1-cm-diam lead collimator just upstream of a 5-mm-square scintillator ($B1$), 38 cm upstream of the target, and a 10-cm-square scintillator ($B2$) with a 5-mm-square hole, 13 cm downstream of $B1$. The incident pion flux was counted by $B1$ in anticoincidence with $B2$. The average pion flux was kept below 10^4 π/s to eliminate the possibility of pileup problems in the detectors. The trigger consisted of a coincidence between $B1$ with any two detectors in the ball, in anticoincidence with $B2$, and in anticoincidence with a 10-cm-square scintillator 86 cm downstream of the target.

Before the final bending magnet in the beam line, a degrader was inserted to minimize protons in the beam. Using pulse heights in scintillator $B1$, the relative fraction of pions in the beam was measured. At incident pion energies of 300 and 500 MeV the pion fraction was measured as 99% and 76%. The pion fraction at 250 and 400 MeV was taken to be 100% from previous measurements made on the P^3 channel.

The targets used in this study were ^{12}C, ^{58}Ni, ^{90}Zr, ^{118}Sn, and ^{208}Pb with thicknesses of 100, 290, 246, 140, and 206 mg/cm^2, respectively. These areal densities were determined with uncertainties of about ±5%. All targets were mounted so that they were centered with respect to the detectors and inclined at an angle of 20° with respect to the incident beam.

B. BGO ball array

A large solid angle detector, the LAMPF BGO ball, was used to detect the reaction products for this study. Detailed information on the BGO ball can be found in Refs. [18] and [19]. The detectors of the array were of pentagonal and hexagonal shape and tightly packed to form a truncated icosahedron of 32 sides. The detectors were distributed about an inner radius of 6.1 cm from the center of the array to the center of each crystal face, and were arranged in six groups centered at laboratory scattering angles of θ = 37°, 63°, 79°, 102°, 116°, and 142°. At the time this experiment was performed only 26 of the detectors were available. Two detectors were missing from the most downstream angles and two were missing from the most upstream side of the ball at conjugate angles. At an incident pion energy of 500 MeV one of the detectors in the ring with the largest scattering angle was not working. The array in this experiment thus covered a scattering angle range of about 20°–160° and a total solid angle of 0.77×4π sr (for 26 detectors). The

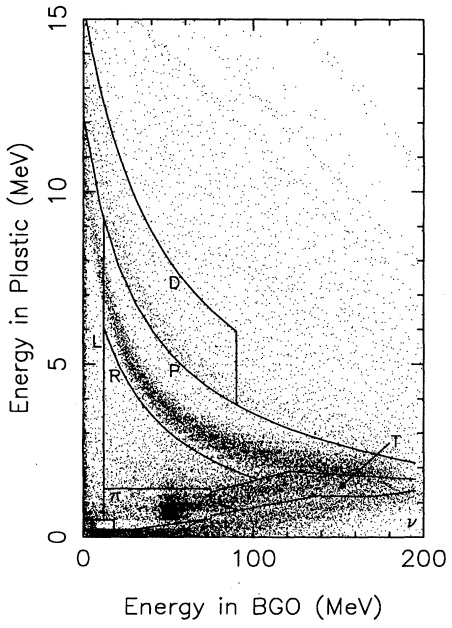

FIG. 1. Pulse heights for the plastic scintillator (ΔE) versus the pulse heights of the BGO scintillator (E), both calibrated for energy deposited (in MeV), obtained from the front three detectors for the $\pi^+ + {}^{12}C$ reaction at an incident pion energy of 500 MeV. Major particle types designated by enclosed regions are (L) low-energy charged particles which stopped in plastic scintillator; (D) deuterons; (P) protons which were stopped by the BGO; (T) "turnaround" protons, which passed through the BGO; (π) pions; (ν) neutral particles, which includes photons and neutrons; and (R) protons which had nuclear interactions in the BGO.

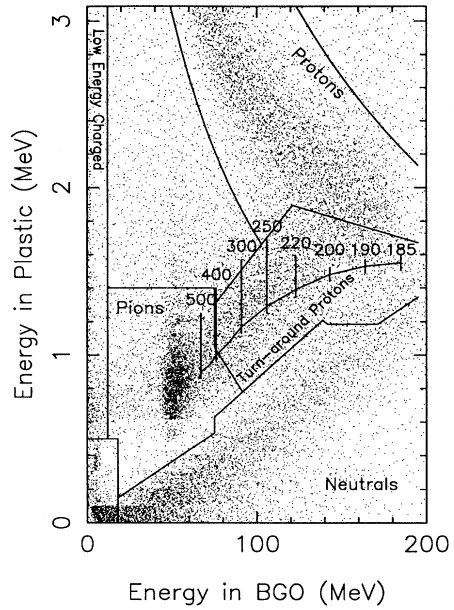

FIG. 2. Enlarged view of Fig. 1. Particle types are labeled as explained in Fig. 1. Minimum ionizing 150 MeV pions form a clump at $E \approx 52$ MeV. Kinetic energies interpolated for "turnaround" protons are shown. The neutral particles do not all have zero energy in the plastic because of pulse shape differences between photons and neutrons, as discussed in the text.

time resolution of the detectors was about 1 ns, sufficient to eliminate hits which came from another beam burst arising from the LAMPF beam 5-ns microstructure.

Each detector consisted of a 3-mm-thick NE102 plastic scintillator glued to the front of a 5.6-cm-thick BGO scintillator. Both scintillators were viewed by a single photomultiplier. Since the decay constant of the BGO scintillator is much longer than that of the plastic scintillator (about 250 ns vs 1.5 ns), the anode signal was time sliced to provide a ΔE and E signal for particle identification. An example of the output signal of the plastic scintillator (ΔE) versus the output signal of the BGO scintillator (E) is shown in Fig. 1, calibrated for energy as described in the next section. The events shown in Fig. 1 were obtained from the three detectors in the azimuthal ring at $\theta = 37°$ and for the $\pi^+ + {}^{12}\mathrm{C}$ reaction at an incident energy of 500 MeV. The only requirement imposed for that figure was that two of the BGO detectors were hit within the time gate with a valid set of beam counter conditions as noted above. Figure 2 shows the same spectrum with an expanded ΔE scale.

C. Energy calibration of the BGO ball

The energy calibration of the BGO ball was made using two proton coincidences from the $\pi d \rightarrow pp$ reaction at several incident energies of the pion beam. The gain for the output from the plastic scintillator was set to give the correct energy deposited in the plastic scintillator for protons with kinetic energy of 50 MeV. The light output from the plastic scintillator was not linearly proportional to the deposited energy. This can be seen in Fig. 1, where the protons and deuterons appear to be passing through the plastic scintillator at 10.5 and 13 MeV, respectively. For proton kinetic energies above 50 MeV or so the light output of the plastic scintillator was approximately a linear function of the deposited energy [20]. Since the energy deposited in the plastic was relatively small, the observed nonlinearity in the plastic scintillator response did not significantly change the estimate of the total energy of any particle.

At higher energies the total cross section for the $\pi d \rightarrow pp$ reaction decreases and the protons become sufficiently energetic such that they are no longer stopped in the BGO material, making the use of the reaction for calibration problematic. Hence, for incident pion energies above 250 MeV, the turnaround point at 185 MeV and the pion minimizing energy point near 52 MeV were used to provide an energy calibration for the detectors. Runs with lower incident pion energy where the $\pi d \rightarrow pp$ method could be used were interspersed among the higher energy runs to check on the consistency of this calibration procedure.

D. Interpretation of BGO ball pulse heights

The light output of BGO scintillator depends on the temperature of the BGO material. To minimize fluctuations in the temperature of the BGO, a tentlike structure was built to isolate the BGO ball from its surroundings. With this housing in place, pulse heights were found to vary by less than a few percent for the energy calibration runs described below.

As seen in Figs. 1 and 2, a fairly clean separation of the different particle types was obtained. The separation was cleaner for lower energy pions, and for more backward angles. We distinguish seven different regions: low-energy charged particles, deuterons, protons stopped in the BGO, protons passing through the BGO, neutrals, low-energy neutrals, and pions. Pions, protons, and deuterons with kinetic energies less than 7.2, 17, and 23 MeV, respectively, were stopped in the plastic scintillator. These same particles were stopped in the BGO crystals for entering energies of 90, 185, and 280 MeV, respectively. Because of the short distance from the target to the detectors, it was not possible to use time of flight to determine the particle type for charged particles stopped in the plastic, or distinguish between neutrons and gammas. Particles which deposited less than 12 MeV in the BGO scintillator and more than 0.5 MeV in the plastic scintillator were identified as low-energy charged particles.

Pions are minimum ionizing for kinetic energies greater than 150 MeV and deposited about 52 MeV of energy in the BGO scintillator. Pions with energies between 90 MeV and 150 MeV passed through the detectors and deposited between 90 and 52 MeV. Since there was insufficient ΔE resolution to distinguish pions with energies between 90 and 150 MeV from those with energies between 52 and 90 MeV, measuring the pion energy spectrum was not possible. Hence, in this experiment the pions were only counted and no missing mass spectra for elastically or inelastically scattered pions were determined.

Incident pion energies used in this experiment were sufficient to produce protons which passed through the BGO detectors. Unlike the pions, there was sufficient ΔE resolution to distinguish these from lower-energy protons. These protons, which we will call "turnaround" protons, are seen in Fig. 2. The "turnaround" point at 185 MeV is clearly seen and particles in the odd-shape box indicated in Fig. 2 were identified as turnaround protons. Protons with enough energy to pass through the BGO scintillator were scattered only to the forward half of the BGO ball. Therefore, turnaround protons were only identified for detectors at $\theta = 37°$, 63°, and 79°. The shape and location of this cut was determined from previous measurements of the $\pi d \rightarrow pp$ reaction for lower pion energies, where the proton energy was readily determined from kinematics.

The observed energy deposited by the turnaround protons in the BGO scintillator was interpreted in software to yield the kinetic energy appropriate for a proton incident on the BGO material of the detector. The scale shown in Fig. 2 illustrates this interpolation. The energy resolution in the plastic scintillator was not sufficient to completely distinguish turnaround protons from stopped protons in the region of 140–185 MeV deposited in the BGO scintillator. Thus, in the worst case, the energy of a 140 MeV proton could be misinterpreted to be 200 MeV. To ameliorate this effect a cut was made in this "turnaround/stopped" proton region so that approximately half the protons in the region were labeled as a turnaround. The effect of this cut in the region of turnaround/stopped region will be discussed in Sec. III, where we describe the results of this division of events on the missing mass spectra obtained. Here, we simply note that the division was found to have no significant effect on the missing mass spectra obtained.

The energy resolution for turnaround protons worsened with increasing proton energy. Up to about 220 MeV the observed energy decreases about 1 MeV per MeV increase in the proton energy, while at 400 MeV the observed energy decreased 1 MeV per 6 MeV energy increase. Hence the energy resolution was 6 times worse for protons which had 400 MeV entering the BGO crystal than those with energies of 220 MeV.

Neutral particles were identified as events in which a signal appeared only in the BGO scintillator. As seen in Fig. 2, the neutral line was not straight but curved upward to higher ΔE as the total energy deposited increased. While this behavior is not fully understood, most of the higher-energy neutrals were probably due to photons from π^0 decays which would have a fast Cherenkov component; this could explain about one-third of the effect. The rest may be due to either a small fast component of light emission from the BGO scintillator, or interaction of electrons from the shower in the photo-cathode. In any case, the neutrals could be distinguished from protons and, since the neutral energy was not used for the analysis described below, this behavior should have no significant impact on the results reported here. To eliminate photons which arose from nuclear transitions or noise, events were distinguished between neutrals with energy deposited in the BGO material above 18 MeV and those which had less than 18 MeV. However, this distinction did not turn out to be very important in the final results.

The neutron detection efficiency for the BGO scintillators used in this experiment has not been measured. The efficiency was estimated by assuming a neutron-nucleus inelastic scattering [21] led to detection of the neutron. This would predict the maximum efficiency for neutron detection is about 25%. Finally, since the BGO scintillator material in each detector had a thickness of 5 radiation lengths, a photon detection efficiency of nearly 100% was assumed.

E. Consistency tests with $\pi d \rightarrow pp$

Because of the simplicity of its final state and the large empirical database available for it, measurements of the $\pi d \rightarrow pp$ reaction provided a useful tool for determining the magnitude of, and assumptions concerning, a number of corrections. To provide the $\pi d \rightarrow pp$ data, the ^{12}C target and empty target runs were subtracted from the CD_2 target runs. Plots of the total energy of the two protons from the $\pi d \rightarrow pp$ reaction are shown in Fig. 3 for incident pion energies of 150, 200, and 300 MeV. The values of the full width at half maximum of the deuteron absorption peak for each of these energies were found to be 15, 18, and 47 MeV, respectively. The resolution became increasingly worse at higher incident pion energies, principally due to the forward-going protons passing through the BGO scintillator.

Estimates of the reaction loss and missing solid angle corrections were tested using the $\pi d \rightarrow pp$ reaction.

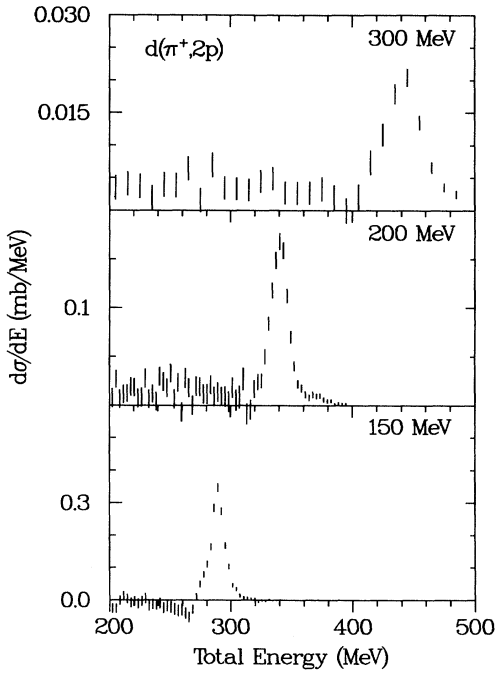

FIG. 3. Observed total energy distribution for two protons for the $d(\pi^+, 2p)$ reaction at various incident pion energies.

For instance, at $T_\pi = 300$ MeV, the peak in Fig. 3 was integrated and, incorporating the measurements of the pion flux and target density noted above, an observed cross section of 0.53 ± 0.04 mb was determined. The 7% uncertainty in the observed cross section includes a 5% uncertainty in the measured pion fraction and a 5% uncertainty in the measured number of incident particles.

The total cross section for $\pi d \to pp$ was then estimated by correcting for losses due to missing solid angle and proton detection efficiency. Not all protons entering the BGO will be identified as such because nuclear reactions by the protons in the detector material can lower their deposited energy enough to move them out of the proton identification bands. From the reaction corrections determined in our previous studies of the $\pi d \to pp$ reaction at lower pion energies, we estimated that, for an incident pion energy of 300 MeV, the correction for reaction losses was 1.7 with an uncertainty of about 10%. The correction for the missing solid angle was estimated using previously measured angular distributions for $\pi d \to pp$ [22]. The solid angle correction was found to be 2.1, also with about a 10% uncertainty.

Applying both corrections, a total $\pi d \to pp$ cross section at an incident pion energy of 300 MeV of 1.9 ± 0.3 mb results, in agreement with the previous measurement of 2.02 ± 0.05 mb [22]. Similar comparisons for other energies indicated that the absolute normalization of the cross sections was accurate to within 10%.

III. OBSERVED CROSS SECTIONS

The goal of this experiment was to measure cross sections and missing energy distributions for pion absorption leading to two or more energetic protons in the final state. Though all events in which a pion was detected in the BGO ball were rejected, unobserved pions in the final state were a source of concern, including the possibility of single charge exchange (CEX) yielding a neutral pion in the final state. The summed energy of the protons was usually not great enough to guarantee absorption, due to, for example, absorption events in which not all particles in the final state were detected, interactions of the outgoing protons in the detectors, pions which reacted in the detectors and were misidentified as protons, or other possibilities. Thus, to estimate the total absorption cross section leading to two or more energetic protons, estimates were made of losses due to incomplete solid angle coverage, reactions of the protons in the BGO, and estimates of the fraction of two proton events which were not due to absorption of the pion.

Because of the possibility that the nonabsorption fraction could be quite large, we will discuss in some detail our evidence for the magnitude of the corrections. We will first outline the general features of the events containing two or more protons, then discuss possible effects of misidentification of the protons and contamination by nonabsorption processes and finally compare the observed missing energy spectra with the predictions of a simple phase space model.

A. Notation

Because of the large phase space covered, large solid angle detectors provide a tool to measure cross sections for many different final states. Such is the case here, and numerous combinations of particles were observed in the BGO ball detector array. In this subsection, we outline the notation used throughout this paper to describe the various cross sections measured, simulated, or inferred. Though somewhat cumbersome, this notation provides an efficient method of summarizing the observables discussed.

We use several subscripts to indicate the restrictions applied, to either the data reduction of events detected by the BGO ball or simulations of the detection system response, in terms of the particular combination of particles required in the final state. The subscript ν indicates a requirement of a neutral particle, which may be a neutron or photon. n or γ denotes a neutron or photon, respectively, in the Monte Carlo simulations. An h indicates a requirement of a "hit" in the ball by any particle, including pions. *None of the cross sections include events which, in the final state, contained an observed pion or two or more neutrals unless so indicated in the subscript.*

Numbers used in conjunction with the foregoing subscripts, such as $2p$, indicate multiplicity requirements for the designated particle. Events with higher multiplicities of the particle than the number indicated in the subscript are excluded from the cross section, but, except for the pion or two neutral exclusion, there is no other restriction on other particles, and the cross sections are in this sense inclusive cross sections. For example, σ_{2p} includes σ_{2pd} and $\sigma_{2p\nu}$, but not σ_{3p} or σ_{4p}.

Notation is also used to indicate the corrections or origin of the given observable. Observed cross sections do not include corrections for missing solid angle or reaction losses, but a superscript of "est" is used to indicate that corrections, discussed in the appropriate section of the text, have been made to obtain the given cross section. A superscript of p indicates data from previous measurements. The subscript "abs" indicates that the cross section has been corrected not only for missing solid angle and reaction losses, but also background from nonabsorption pion events; such cross sections thus represent our estimates of the absolute pion absorption cross sections, and are inclusive cross sections except for the aforementioned exclusion of events with pions or two or more neutrals in the final state.

B. Observed cross sections

The observed cross sections σ_{2p}, σ_{3p}, σ_{pd}, σ_{2pd}, and $\sigma_{2p\nu}$ (the last two, as indicated above, are subsets of σ_{2p}) are given in Table I. The statistical uncertainties are generally about 1%. Because the uncertainties in pion flux and target thickness amount to about 10%, we have rounded all results to two significant figures and omitted the statistical error. The observed $4p$ cross sections are always small and never more than 10% of the observed $3p$ cross section. We have listed two cross sections which include a deuteron, σ_{pd} and σ_{2pd}, to indi-

TABLE I. Observed cross sections measured in this experiment for events with two protons (σ_{2p}), three protons (σ_{3p}), a proton and a deuteron (σ_{pd}), two protons and a deuteron (σ_{2pd}), and two protons and a neutral ($\sigma_{2p\nu}$). σ_{2pd} and $\sigma_{2p\nu}$ are subsets of σ_{2p}. Because the systematic normalization uncertainty is about 10%, while statistical errors are of order 1%, we have rounded results in this and later tables to two significant figures and omitted that statistical error.

T_π (MeV)	Nucleus	σ_{2p} (mb)	σ_{3p} (mb)	σ_{pd} (mb)	σ_{2pd} (mb)	$\sigma_{2p\nu}$ (mb)
250	^{12}C	25	4.0	4.4	1.9	3.3
250	^{58}Ni	96	16	19	6.5	8.8
250	^{90}Zr	97	14	23	6.8	8.5
250	^{118}Sn	130	18	36	9.7	9.8
250	^{208}Pb	140	14	39	8.7	9.8
300	^{12}C	24	4.5	4.4	1.9	4.4
300	^{58}Ni	110	21	22	8.5	14
300	^{90}Zr	110	20	27	9.2	13
300	^{118}Sn	120	19	32	10	13
300	^{208}Pb	170	24	49	13	18
400	^{12}C	18	3.8	3.3	1.6	5.0
400	^{118}Sn	140	30	39	16	23
400	^{208}Pb	160	29	50	17	24
500	^{12}C	18	4.0	3.4	1.7	5.9
500	^{58}Ni	120	34	26	14	27
500	^{90}Zr	130	34	36	17	28
500	^{118}Sn	150	38	45	21	30
500	^{208}Pb	240	52	76	30	42

cate that final states including an energetic deuteron are significant. However, we see that the observed $2p$ cross sections are dominant and most of the discussion in this subsection will concern them.

Events containing two or more neutrals were mainly due to charge exchange, as discussed in the Appendix. Using the techniques and assumptions described there, cross sections including pions, two neutrals, or various combinations of low-energy particles were also measured. Some of these are listed in Tables III and IV. Because of the trigger requirement of two detectors being hit, pion elastic cross sections were not measured, but the results in Tables III and IV do provide a measure of the total reaction cross section, using the observed cross section for two or more detectors hit. This latter cross section is listed as $\sigma_{\geq 2h}$ in Table IV. A comparison with the total reaction cross section of Ref. [1] is also given at 250 and 300 MeV. Our observed $\sigma_{\geq 2h}$ is about $50 \pm 10\%$ of the reaction cross section at 250 and about $60 \pm 10\%$ at 300 MeV. For ^{12}C at 400 and 500 MeV [23], $\sigma_{\geq 2h}$ is 60% and 70% of the reaction cross section.

C. Missing energy spectra

The observed missing energy spectra for $2p$ and $3p$ events with targets of ^{12}C, ^{58}Ni, and ^{208}Pb at various incident energies are shown in Figs. 4–9, with missing energy defined as the sum of the incident pion kinetic energy plus the pion mass minus the summed energy of all observed protons. We have not included the energy

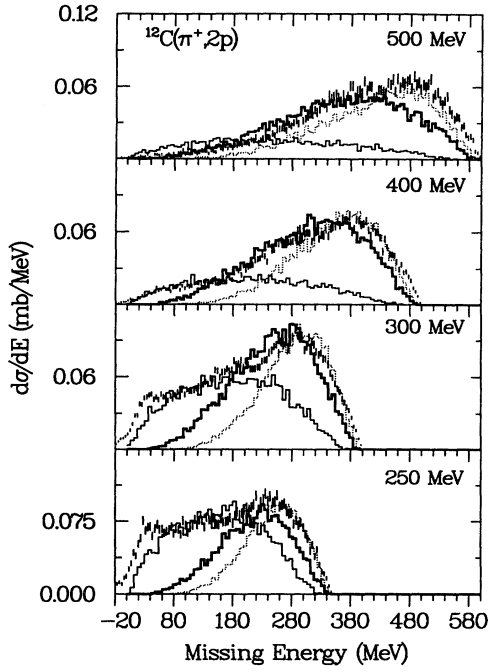

FIG. 4. Observed missing energy distributions for the ^{12}C(π^+, $2p$) reaction at various incident pion energies. Also shown are histograms for the calculated missing energy distributions for $2pn$ (light line), $2p2n$ (dark line), and $2p3n$ (dotted line) final states from a Monte Carlo simulation with an arbitrary normalization, as explained in Sec. IV.

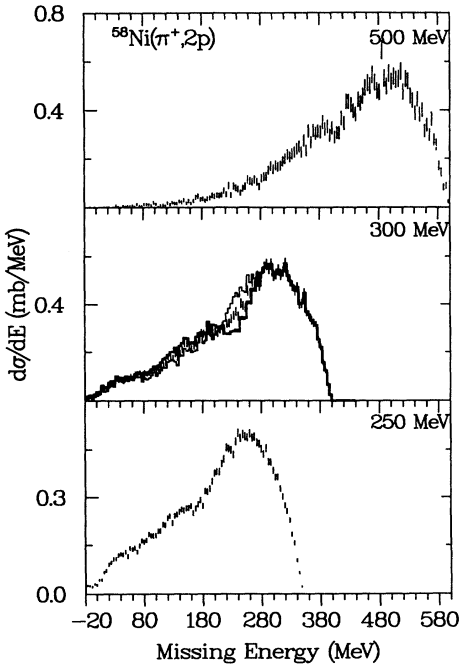

FIG. 5. Observed missing energy distributions for the ^{58}Ni(π^+, $2p$) reaction at various incident pion energies. Also shown are distributions at 300 MeV indicated with light (dark) lines where all protons in the "turnaround/stopped" region were given energies appropriate for stopped ("turnaround") protons, as described in the text.

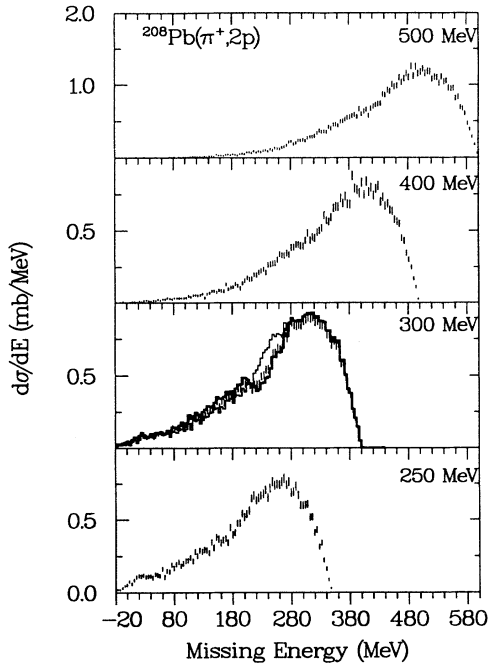

FIG. 6. Observed missing energy distributions for the ^{208}Pb(π^+, 2p) reaction at various incident pion energies. The light and dark histograms shown for 300 MeV are as described in the caption for Fig. 5 and discussed in the text.

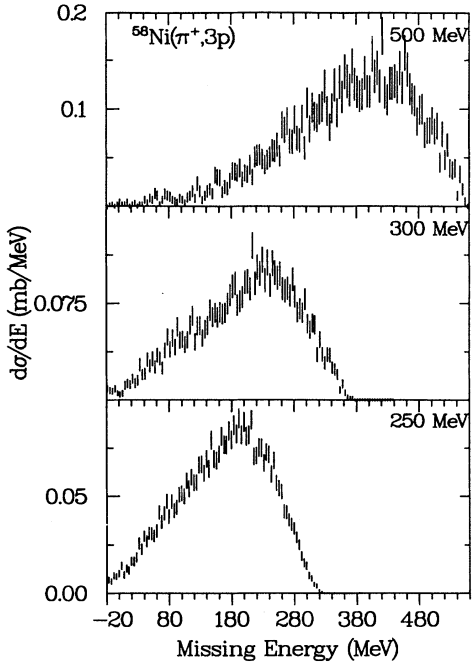

FIG. 8. Missing energy distributions for the observed 3p cross section from the ^{58}Ni(π^+, 3p) reaction at various incident pion energies.

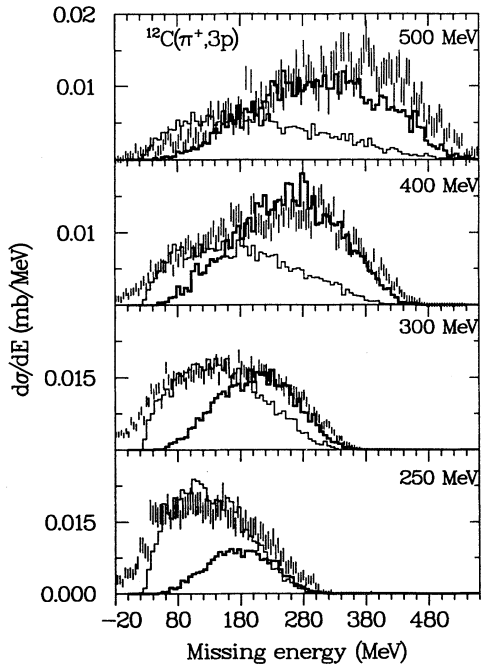

FIG. 7. Observed missing energy distributions for the ^{12}C(π^+, 3p) reaction at various incident pion energies. The histograms are the calculated missing energy distributions for 3pn (light line) and 3p2n (dark line) final states from the simulation explained in Sec. IV. The curves have an arbitrary normalization.

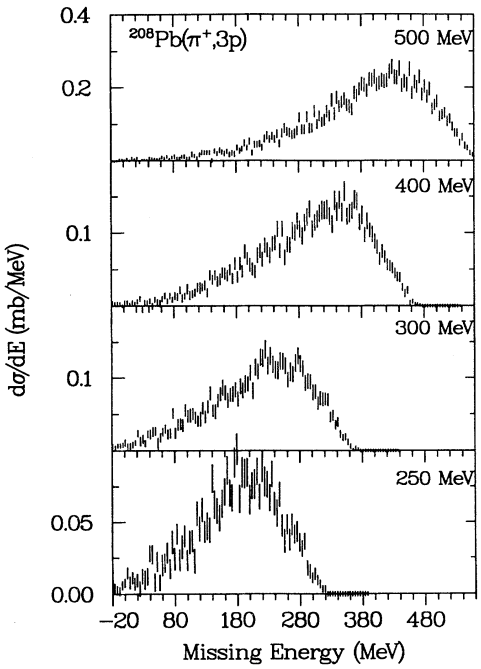

FIG. 9. Missing energy distributions for the observed 3p cross section from the ^{208}Pb(π^+, 3p) reaction at various incident pion energies.

of deuterons or other particles, in order to make more reliable comparisons with the simulations discussed below. As is easily seen from Figs. 4–6, the bulk of the observed $2p$ cross section has a missing energy greater than the pion mass energy of 140 MeV, with the fraction increasing for both increasing incident pion energy and increasing mass.

Three physical processes can contribute to the large missing energy region: absorption on more than two nucleons with one or more nucleons unobserved, absorption with initial state and/or final state interactions leading to one or more energetic but unobserved nucleons, and nonabsorption events with an unobserved pion. The corrections and assumptions relevant to interpreting the missing mass spectra for the first two of these processes were investigated using simulations, as described in the next section, while the last process is discussed here, along with a discussion of corrections made for misidentified pions and protons in the final state.

1. Corrections for pion inelastic and charge exchange

Pion inelastic scattering and CEX events can contribute to the observed $2p$ spectrum. We have estimated their contributions to the observed $2p$ spectrum by first determining the total cross sections for inelastic and CEX reactions, as detailed in the Appendix. We then estimated the fraction which contributed to the $2p$ spectrum but was not rejected by either observing a pion or the two photons from π^0 decay. While the determination of these cross sections is discussed in detail in the Appendix, here we note that the total cross sections for inelastic and CEX reactions estimated from this experiment were in reasonable agreement with previous data, and at energies where no previous data existed the cross sections measured here follow the trend from lower energies.

From our measurements, the contribution to the observed $2p$ cross section from pion inelastic scattering was found to be less than 5% for all nuclei and at all energies. The CEX reaction contributed less than 12% to the observed $2p$ cross section for all nuclei and at all energies, except for ^{12}C at 400 and 500 MeV where the CEX contribution was 15% and 26%, respectively. In determining the final total absorption cross section discussed in the next section, these contributions from nonabsorption events were subtracted.

2. Corrections for particle misidentification

Consideration was given to several processes within the BGO material which could give rise to misidentification of particles. Possible misidentification due to pion interactions in the detector material were investigated, the aforementioned energy ambiguity in the turnaround/stopped proton region, confusion of high-energy pions and protons, and proton interactions resulting in improper incoming energy assignment. These are discussed here in turn.

A scattered pion can interact in the BGO in such a manner as to give a signal which could be interpreted as a high-energy proton. Based on the cross sections of Ref. [1], about 30% of the pions at 165 MeV underwent an inelastic reaction, and 24% of them at 300 MeV did. If the energy loss of the pion was less than about 30 MeV, or if the pion lost most of its energy in a transfer to one or more neutrons either directly or through final state interactions, it would likely still be identified as a pion. Even most events with greater energy loss (including absorption in the BGO) would not be identified as protons, since most of these will give a ΔE signal which is too low, or an energy which does not fall in the relatively narrow range allowed for the turnaround protons. For the detectors backward of 90°, no confusion of pions and protons due to pions interacting in the detector should occur since the turnaround region for those detectors was essentially empty for proton events. Further, in these backward angle detectors, the pion band was not seen at higher energies for the ΔE corresponding to a pion. This, coupled with the results on pion cross sections detailed in the Appendix, indicates that such interactions do not contribute significantly to the observed two proton cross sections; thus, no corrections were made for such effects.

As mentioned earlier, a shift in the missing energy distribution could occur if turnaround protons were misidentified as stopped protons, and thus assigned too low an energy. To interpret this region, we indicated above that a cut was made in this turnaround/stopped region for the proton curve such that about half the events in that region were labeled turnaround protons, while the remaining protons were assigned energies appropriate to protons stopping in the rearmost part of the detector material. If this procedure resulted in a great number of serious erroneous energy determinations, the missing energy distributions would be correspondingly skewed. Simple considerations would suggest that this ambiguity should have minor effects on the inferred missing energy distributions. For example, if the interpolated energies for these protons were off by 5%, then the turnaround protons would have energies incorrect by at most 25–30 MeV, which should have a negligibly small impact on the missing energy distribution.

To confirm this assumption, the ambiguity in the turnaround/stopped region was investigated by using different assumptions for treatment of this region and observing the changes found in the missing mass spectra. The histograms in Figs. 5 and 6 at incident pion energy of 300 MeV are the $2p$ missing energy distributions found using different assumptions for the treatment of events in the turnaround/stopped region. If the assumption is made that all the events in the region were stopped protons, the histogram indicated by the light line results. If, conversely, all such protons are assigned energies interpolated for turnaround protons, the dark line indicates the resulting missing energy distribution. Both missing energy distributions are seen to lie almost within the error bars of the missing energy distribution in which about half of the protons with energies above 140 MeV were identified as stopped protons, the prescription we have employed. Thus, the procedure described above for treating the ambiguity in this region has no significant

detrimental effect on the missing energy distributions discussed below.

As can be seen in Fig. 2, the deposited energy of turnaround protons approaches that for pions as the proton kinetic energy increases. For this work, a minimum energy deposit in the BGO material of 75 MeV for turnaround protons has been assumed, which limits the interpolated maximum proton energy to around 410 MeV and the minimum scattered pion kinetic energy to about 100 MeV. For pion beam energies below 300 MeV this limitation was not important. Protons from the $\pi d \rightarrow pp$ reaction with a scattering angle of $\theta = 20°$ had kinetic energies below 325 MeV, and, even taking into account Fermi motion in the nucleus, proton energies larger than 410 MeV were unlikely.

For incident beam energies of 400 and 500 MeV, however, proton kinetic energies of 409 and 494 MeV, respectively, were expected for the same reaction. For these energies the cutoff at 410 MeV in proton kinetic energy would cause some high-energy protons to be identified as pions. Changing the assumed minimum energy deposition to 65 MeV would increase the upper limit for interpolated proton kinetic energies of 525 MeV, although some pions would then be incorrectly identified as protons. The effects of varying the assumed minimum energy deposit were tested for the 500 MeV incident pion energy data, where the effects should be the largest. The results of that investigation indicated that the observed inclusive two-proton cross section increased as would be expected, but by only about 0.5% for all nuclei. Thus, the exact placement of the cutoff is of little significance. (We also note that this indirectly supports the contention that pion interactions in the BGO are not a significant factor.)

Protons undergoing nuclear reactions in the detector might still be identified as protons, but with the incorrect energy. In the turnaround region the observed energy of such a proton could be greater or less than the energy of a nonreacting proton, depending on the reaction. A proton with an energy less than 185 MeV undergoing a nuclear reaction will deposit less than its full energy. If that difference is more than about 50 MeV, it will no longer be identified as a proton. Otherwise, it will be identified as a proton but with some energy unobserved, resulting in a downward shift in missing energy of up to 50 MeV. This is much less than the difference between the peak of the missing energy spectrum and zero missing energy. Thus even if every event contained a proton which had undergone a nuclear reaction but was still identified as a proton, the missing energy spectrum would still not peak at low missing energy. In contrast to protons below 185 MeV, nuclear interactions by the protons which have enough kinetic energy to pass through the BGO scintillator are likely to lead to more energy deposited, due to the higher differential energy loss of the original proton, plus the energy of any additional protons knocked out of the nucleus. However, these will have a low-energy deposit in the plastic and generally fall outside the turnaround proton cuts. We also estimate that less than 25% of the high-energy protons should undergo any inelastic nuclear reaction [21]. We conclude that the general shape of the spectrum is not due to misidentification of the proton or its energy.

IV. TOTAL ABSORPTION CROSS SECTIONS

A. Simulations of corrections to observed cross sections

As mentioned in the preceding sections, most of the observed $2p$ cross section appears to be due to absorption. To estimate the total absorption cross section for only two protons in the final state, the observed two-proton cross sections must be corrected for missing solid angle, losses due to nuclear reactions in the detectors, and the fraction of observed two-proton events which contained one or more undetected protons. Similar considerations apply to obtaining the total absorption cross section for final states with only three protons from the observed cross sections with three protons detected in the ball. As discussed above, for the $\pi d \rightarrow pp$ reaction, the reaction and solid angle corrections are straightforward, only two protons can arise in the final state, and estimates can be made which are easily confirmed by comparison with other experiments.

For heavier nuclei, however, there is no unambiguous way of making these corrections. For this work the angular and energy distributions of the nucleons in the final state were assumed to be reasonably described by multinucleon phase space. The characteristics of final states with various numbers and combinations of protons and neutrons were studied and compared to the characteristics of the data in order to determine which final states best described the data. From those comparisons, estimates of the total absorption cross section leading to only two, only three, or more protons were made. These simulations revealed that, due to the large solid angle coverage, relatively low proton detection threshold, and high efficiency for proton detection, the correction from the observed $2p$ cross section to total absorption cross section was relatively insensitive to the final state assumed in the simulations.

The basic event generator used was the Monte Carlo phase space program FOWL [24], which in this work was used to simulate the absorption of a pion on a cluster of nucleons bound by 8 MeV/nucleon. The use of a cluster to simulate the absorption mechanism does not imply necessarily that the underlying pion absorption mechanism was dominated by a process involving all the nucleons of the cluster; instead, the cluster approach simply provided a means of assessing the overall detection probability. A number of final states containing at least two protons were simulated: $2pn$, $2p2n$, $2p3n$, $3pn$, and $3p2n$. In each case the full phase space distributions of the particles were used.

After generation of each event, the response of the BGO ball detectors for the protons and neutrons was also simulated. For those protons which underwent a nuclear reaction, an estimated energy loss was predicted and tested to determine whether the proton remained in the proton band of the ΔE vs E plot. These estimates were based on our previous studies of the $\pi d \rightarrow pp$

reaction at lower pion energies. The neutron detection efficiency was assumed to be zero for neutrons below 30 MeV, to rise linearly from zero to 25% for neutrons between 30 and 100 MeV, and constant at 25% above 100 MeV.

After this estimation of the detection probability for each particle was made, the following characteristics of the simulated final states were examined: the ratio of events generated to those events in which only two protons are detected, the ratio of three detected protons to two detected protons, and the observed missing energy spectrum for events with two or three detected protons. These ratios are summarized in Table II for the various final states noted above. Also estimated, but not listed, were the ratios of observed $2p2n$ to observed $2p$ final states. These were found to vary from 0.005 at 250 MeV to 0.02 at 500 MeV, indicating that the observed $2p2\nu$ cross section had little contribution from $2p2n$ events and was mainly due to charge exchange.

The correction factors required for the $\pi d \rightarrow pp$ were found using the angular distributions from the parametrization of Ref. [25]. These are listed in Table II under the column labeled "$d(\pi^+, 2p)$." The ratio of the total number of events to the number of events with two detected protons generated in the Monte Carlo simulation was used as the correction factor for the observed $2p$ cross section to get the total cross section for each final state. For example, at 250 MeV for the column labeled $3p2n$, which corresponds to the reaction $\pi^+ppnnn \rightarrow pppnn$, the observed $2p$ cross section was predicted by these simulations to be only 40% (1/2.5) of the total cross section while the code predicted that the observed $3p$ cross section would be 41% of the observed $2p$ cross section. In other words, if the total cross section for this reaction were 100 mb, the code would have predicted an observed cross section σ_{2p} of 40 mb of which 16.4 mb would be observed $3p$ cross section.

It is clear from Table II that the correction factor from the observed two proton cross section to total absorption cross section was not very sensitive to the final state simulated. For instance, at 250 MeV, the $2p$ correction factor found for the different clusters ranges from 2.5 to 3.3. The difference between the minimum and maximum correction factors and the simple average of the two is generally 15–25 %. Since (1) the factors were approximately equal, (2) there was no unambiguous method to weight the various correction factors, and (3) the variation was about the same magnitude as the various uncertainties in the simulation, a simple average value from the factors in Table II was used as an estimate for the correction for missing solid angle and reactions.

TABLE II. A Monte Carlo prediction of the ratio of the total absorption cross section to the observed two-proton cross section for the deuteron [column labeled $d(\pi^+, 2p)$] and various combinations of nucleon clusters in the final states. It is the correction factor for missing solid angle and reaction losses in the BGO ball for each nucleon cluster. For the $3pn$ and $3p2n$ nucleon clusters the value after the slash is the Monte Carlo prediction for the ratio of the observed $3p/2p$ cross section. See Sec. IV for a description of the simulation.

T_π	$d(\pi^+, 2p)$	$2pn$	$2p2n$	$2p3n$	$3pn$	$3p2n$
250	3.5	3.1	3.1	3.3	2.5/0.45	2.5/0.41
300	3.6	3.3	3.1	3.3	2.5/0.44	2.5/0.41
400	3.8	3.6	3.4	3.3	2.5/0.41	2.5/0.42
500	3.9	4.3	3.8	3.6	2.6/0.36	2.6/0.39

B. Total absorption cross sections

To obtain the total absorption cross section leading to two or more energetic protons in the final state, the associated missing mass spectra were integrated. The observed σ_{2p} cross sections were integrated over two energy regions. The first region, designated LE, corresponded to the portion of the spectra which was below a cutoff energy T_c, where T_c was equal to 100 MeV plus the two-proton separation energy. The remaining higher missing energy portion, labeled HE, was integrated for all missing energy above T_c. The predicted contribution to observed σ_{2p} of nonabsorption events was subtracted from the HE integrated cross section since nonabsorption events should contribute primarily to that missing energy region.

In Table III the integrated cross sections for the two missing energy regions are listed as σ_{2p}(LE) and $\sigma_{2p}^{\rm est}$(HE). These integrated cross sections were then adjusted according to the corrections for missing solid angle and reactions as noted above. In particular, the observed $2p$ LE cross sections were multiplied by the deuteron absorption cross section correction factor, while the observed $2p$ HE cross sections were multiplied by the average of the maximum and minimum correction factors at each pion energy as detailed in the previous subsection. Both integrated absorption cross sections are listed in Table III as $\sigma_{\rm abs}^{\rm est}$(LE) and $\sigma_{\rm abs}^{\rm est}$(HE) and plotted in Fig. 10 for all targets and incident pion energies.

The sum of the two missing energy regions gives the estimated total absorption cross section leading to two or more protons ($\sigma_{\rm abs}^{\rm est}$). The values are plotted in Fig. 11(a) and listed in Table III. Based on the uncertainties mentioned above for the pion flux, target density, and all correction factors noted above, the estimated cross sections possess uncertainties of about 20% for 250 MeV–400 MeV, and 30% at 500 MeV, except for ^{12}C, with an uncertainty of 45%. The main sources of uncertainty are the subtraction of the contribution of nonabsorption events from observed σ_{2p} and the phase space corrections.

The predicted ratio of $3p/2p$ can be compared to the observed values. After correction of the observed $2p$ cross sections for nonabsorption events [the sum of σ_{2p}(LE) and $\sigma_{2p}^{\rm est}$(HE) listed in Table III], the ratio of observed $3p$ to $2p$ is 10–20 % at 250 MeV to 20–35 % at higher energies. The ratios are listed in Table III. In the Monte Carlo simulation for final states with three protons, the ratio of observed $3p$ to $2p$ is predicted to be about 40%, and of course, 0% for the final states without three protons in the final state (see Table II). This indicates that between 1/3 and 2/3 of the total absorption cross section, depending on the nucleus and pion energy, leads to three-proton final states.

The observed $3p$ cross sections are listed in Table I. As

TABLE III. Total cross sections and ratios determined from integrations of the observed missing mass spectra measured in this experiment, corrected for reactions and missing solid angle as described in the text. The notation and the LE and HE integration limits are described in the text. (σ^{p}_{abs}) are from Ref. [1]. The uncertainty for σ^{est}_{abs} is estimated at about 20% for π energies up to 400 MeV and 30% for 500 MeV for all nuclei except ^{12}C where the error is 45%.

T_π (MeV)	Nucleus	σ_{2p}(LE) (mb)	σ^{est}_{2p}(HE) (mb)	$3p/2p$	σ^{est}_{abs}(LE) (mb)	σ^{est}_{abs}(HE) (mb)	σ^{est}_{abs} (mb)	σ^{p}_{abs} (mb)	σ^{est}_{3p} (mb)
250	^{12}C	8.5	15	0.17	30	43	73	95±22	25
250	^{58}Ni	17	76	0.17	60	220	280	411±70	99
250	^{90}Zr	15	80	0.15	53	230	280	440±105	87
250	^{118}Sn	20	107	0.14	70	310	380		112
250	^{208}Pb	19	120	0.10	67	340	400	854±166	87
300	^{12}C	5.5	17	0.20	20	49	69	64±27	27
300	^{58}Ni	12	93	0.20	43	270	310	320±62	128
300	^{90}Zr	11	99	0.18	40	290	330	390±90	122
300	^{118}Sn	11	105	0.16	40	300	350		116
300	^{208}Pb	13	150	0.15	47	450	500	618±170	146
400	^{12}C	1.5	13	0.26	5.7	39	45		24
400	^{118}Sn	2.9	120	0.24	11	390	400		189
400	^{208}Pb	2.7	150	0.19	10	460	470		183
500	^{12}C	0.43	11	0.36	1.7	37	39		29
500	^{58}Ni	0.76	96	0.35	3.0	330	330		224
500	^{90}Zr	0.59	110	0.31	2.3	380	380		252
500	^{118}Sn	0.64	130	0.29	2.5	440	440		343
500	^{208}Pb	0.54	210	0.25	2.1	710	710		378

was done for the observed $2p$ cross sections, Monte Carlo simulations were done for $3pn$, $3p2n$, $3p3n$ final states with phase space kinematics to predict the ratio of the total number of events generated to the number of events with only three detected protons. This ratio was used to give a correction factor for each final state. The mean correction factor for the three final states was found to be 6.2, 6.1, 6.3, and 7.0 for incident pion energies of 250, 300, 400, and 500 MeV, with the individual correction factors for the different final states being within 15% of the simple average value at each pion energy. Again, this variation is probably smaller than the overall uncertainty of the simulation, and so we have simply used the mean value of the correction factor to estimate the total cross section for absorption leading to three energetic protons in the final state and an error of 25% is assumed. The estimated total $3p$ cross sections (σ^{est}_{3p}) are plotted in Fig. 11(b), and listed in Table III. This cross section is part of the estimated σ^{est}_{abs} cross section. As a consistency check, the Monte Carlo simulation can be used to estimate the contribution of the three proton final states to the observed two proton cross sections. That contribution can be subtracted from the two proton cross section, which can then be corrected according to the final states without three protons. The sum of the corrected two and three proton cross sections is nearly identical to just taking the mean of minimum and maximum correction factors, as described above, and applying it to the two proton cross section, i.e., without attempting to directly separate the two and three proton final states.

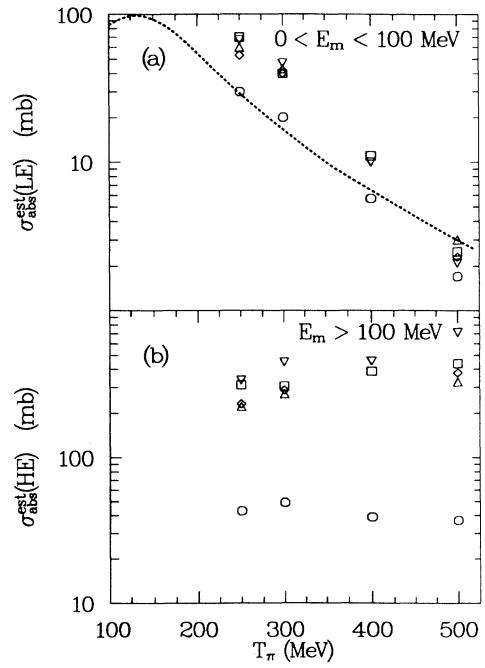

FIG. 10. The estimated two-proton inclusive cross sections (a) σ^{est}_{abs}(LE) and (b) σ^{est}_{abs}(HE) for targets of ^{12}C (○), ^{58}Ni (△), ^{90}Zr (◇), ^{118}Sn (□), ^{208}Pb (▽). The dashed line is from a parametrization of the $\pi d \rightarrow pp$ total absorption cross by Ritchie [25] normalized to the σ^{est}_{abs}(LE) data.

The simulated missing energy distributions can be compared with the observed distributions. Shown in Fig. 4 are the simulated missing energy distributions for the $2pn$, $2p2n$, and $2p3n$ final states. Each curve was normalized such that its maximum was not greater than the data; this means that they collectively do not sum to equal the data. In Fig. 7 are the predictions for the $3pn$ and $3p2n$ final states compared with the $3p$ missing energy distribution. As both the incident pion energy and target mass increase, the number of nucleons required in the phase space also increases. The three-body final state, $2pn$, is seen to populate the low-missing-energy

part of the spectrum, and clearly decreases in importance for both increasing mass and increasing incident pion energy. The peak of the spectrum is shifted to greater missing energy than expected from the ratio of observed protons to total nucleons in the cluster. This results from the fact that the higher-energy protons tend to be more forward going, and are thus more likely to be unobserved, and a higher-energy proton is more likely to undergo a nuclear reaction and thus not be identified as a proton. Both effects push the spectrum to larger missing energy, and both become more important as the pion energy increases. Thus, although the missing energy is great, it appears to be consistent with the energy being shared by only three to five nucleons, with one to three of the nucleons being unobserved.

The total cross section for absorption leading to two protons and one or more energetic neutrals can be estimated from the $\sigma_{2p\nu}$ cross section. This provides a test of the consistency of the procedures used above for the proton spectra. However, the cross sections determined from $2p\nu$ events are considerably more uncertain than the previous estimates due to our limited knowledge of the neutron detection efficiency, the neutron energy spectrum, and the contribution of charge exchange events. But, using the simulation discussed above, values were obtained which were consistent with the values determined from the observed two and three proton cross sections, and in particular were consistent with most of the $2p$ final states containing one or more energetic neutrons.

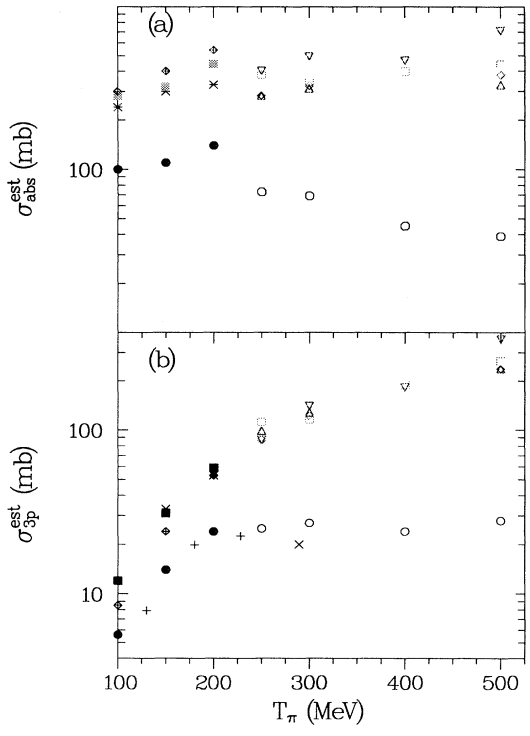

FIG. 11. Plotted are the estimated total absorption σ^{est}_{abs} in part (a) and in part (b) the total three-proton cross sections σ^{est}_{3p} are plotted. The data from this paper are for incident pion energies between T_π 250 to 500 MeV and the symbols denoting the nuclei are the same as Fig. 10. Also shown in the parts (a) and (b) of the figure are data from a previous experiment [26] using the BGO ball where incident pion energies were between 100 to 200 MeV and the symbols for the nuclei are : ^{12}C (solid circle), ^{58}Ni (asterisk), ^{118}Sn (solid squares), and ^{208}Pb (diamond with a cross inside). Shown in part (b) of the figure are the $^{12}C(\pi^+, 3p)$ data from Refs. [17] and [30] which are represented by a cross and a ×, respectively.

V. DISCUSSION OF THE DATA

A. Comparison to other experiments

Data taken with the BGO ball in a similar setup for incident pion energies between 50 and 200 MeV for many of the same targets as in this study have been published previously [26]. The estimated absorption cross sections leading to two or more energetic protons σ^{est}_{abs} from that experiment are plotted in Fig. 11(a). There is a smooth agreement between the two data sets.

The total absorption cross sections measured by Ashery *et al.* [1] are compared to our estimates in Table III. At an incident energy of 250 MeV the σ^{est}_{abs} for ^{12}C, ^{58}Ni, and ^{90}Zr are lower than the previously measured total absorption cross section and for ^{208}Pb σ^{est}_{abs} is about half the total absorption cross section given by Ashery *et al.* Earlier measurements below 200 MeV with the BGO ball found a similar discrepancy between σ^{est}_{abs} and the total absorption cross section, a disagreement which became worse with increasing mass, but descreased as the incident pion energy increased. If we assume that the previous measurements are correct, this discrepancy could be explained by a reaction product component in pion absorption, consisting of low-energy protons (less than 22 MeV) and low-energy neutrons, which is undetected in our $2p$ measurements. As the incident pion energy increases, the energy of this component may increase and less of it might be missed in the measurement of the $2p$ cross section. By an incident energy of 300 MeV the σ^{est}_{abs} cross sections measured here are consistent with those of Ashery *et al.*, as seen in Table III. Thus, for incident pion energies above 300 MeV, σ^{est}_{abs} appears to be a good measure of the total absorption cross section.

Exact comparison of the results obtained here with those from other experiments is difficult because of the significant differences in experimental techniques. Altman *et al.* [27] used small solid angle detectors set at quasideuteron kinematics to measure the $(\pi^+, 2p)$ cross section at an incident energy of 165 and 245 MeV. For ^{12}C, Fe, and Bi at 245 MeV cross sections of approximately 11, 24, and 29 mb, respectively, were obtained. These cross sections were associated with the quasideuteron absorption mechanism unperturbed by initial and/or final state interactions.

To measure a quantity similar to the data of Altman *et al.*, the $2p$ missing energy distributions were integrated from 0 to 50 MeV plus the two proton binding energy and multiplied by the quasideuteron correction factor. For ^{12}C, ^{58}Ni, and ^{208}Pb at an incident energy of 250 MeV the cross sections were 17, 27, and 28 mb, respectively. Therefore, our ^{12}C cross section is about 1.5 times larger

than Altman *et al.*, while the nickel and lead data are about equal to the data of Altman *et al.* Hyman *et al.* [28] measured the $^{16}O(\pi^+, 2p)$ cross section at incident energy of 165 MeV and found a cross section a factor of 2.3 larger than Altman *et al.* Measurements of the $^{58}Ni(\pi^+, 2p)$ cross section by Burger *et al.* [29] at incident energy of 160 MeV were about 2 times larger than the cross section measured by Altman *et al.* Measurements of $(\pi^+, 2p)$ cross sections on ^{12}C, ^{58}Ni, and ^{208}Pb at an incident energy of 150 MeV with the BGO ball [26] were also 2–3 times larger than the data of Altman *et al.* There thus seems to be a normalization problem in the data of Altman *et al.* at 165 MeV, but at an incident energy of 245 MeV their results, with the possible exception of ^{12}C, are consistent with our measurements.

The estimated inclusive $3p$ cross sections are plotted in Fig. 11(b) along with earlier $3p$ cross sections measured with the BGO ball for incident pion energies below 200 MeV [26]. Also plotted in Fig. 11(b) are the $^{12}C(\pi^+,3p)$ cross section measurements by Tacik *et al.* [17] at incident pions energies of 130, 180, and 228 MeV and Brückner *et al.* [30] at an incident energy of 289 MeV. The data of Tacik *et al.* agrees with the magnitude and shape of the excitation function for data taken with the BGO ball. The data point of Ref. [30] at $T_\pi = 289$ MeV is lower than the present data, but within error bars.

In the $Cu(\pi^+, p)$ experiment at incident pion energy of 476 MeV Golubeva *et al.* [31] extracted from the proton angular distributions, in a manner similar to the work of McKeown *et al.* [32], that five nucleons share the total pion energy. This is consistent with our phase space description of the data.

B. Comments on the data

The analysis above demonstrates that the missing energy spectra have a large fraction of events with large missing energy. The simulations suggest that the shape of the spectra can be described by processes distributing the energy among three to five nucleons, although due to initial and final state interactions this does not directly indicate the number of nucleons directly involved in the absorption. The cross sections for absorption appear to remain large as the energy increases above the Δ resonance, with only the cross section for carbon decreasing significantly. If we assume that σ_{abs}^{est} describes accurately the total absorption cross section, absorption represents about one-fifth of the total reaction cross section for ^{12}C, even at 500 MeV (see Tables III and IV). A comparison of our data with the total cross sections reported by Carroll *et al.* [33] and in Ref. [23] would indicate that the absorption cross sections are in the range of 10%–20% of the total cross sections, still a significant fraction of the total cross section, but less than near the peak of the $\Delta(1232)$ resonance.

Plotted in Fig. 10(a) (dashed line) are the total cross sections for the $\pi d \rightarrow pp$ reaction, normalized to the current data, from the parametrization by Ritchie [25]. These cross sections drop by a factor about 10 between $T_\pi = 250$ and 500 MeV. The energy dependence of the cross sections for heavy nuclei obtained here by integrating over missing energy less than 100 MeV are seen to have an energy dependence similar to the $\pi d \rightarrow pp$ reaction. This is suggestive evidence that QDA is largely responsible for the cross section with missing energy less than 100 MeV.

Determination of the origin of the large missing energy region, in particular the relative contribution of ISI/FSI, QDA, and multinucleon mechanisms, is a difficult process, and beyond the scope of this paper. However, they do not appear to exhibit the energy dependence of the deuterium cross section, in contrast to the low-missing-energy region. Understanding the energy dependence and underlying mechanisms of pion absorption which lead to large missing energy will represent an area of intense interest in the future. Experiments which can further illuminate the phenomena associated with that region of the missing energy spectra will be crucial in further advancing our understanding of pion absorption.

VI. CONCLUSIONS

The first systematic measurements of pion absorption on a wide range of nuclei for pion energies above 300 MeV have been presented. These data provide a large body of empirical data which should permit tests of theories of the pion absorption mechanism. The total absorption cross sections remain large and approximately constant above 250 MeV. The energy dependence of the absorption cross section derived from the low-missing-energy region is markedly similar to that of $\pi d \rightarrow pp$, most likely indicating the dominance of quasideuteron absorption for that region.

The overall importance of quasideuteron absorption, the significance of initial state interaction, and the role played by multinucleon absorption mechanisms in the pion absorption process on heavy nuclei above the $\Delta(1232)$ resonance remains unclear. A full understanding of these data will require more complete theoretical calculations which include both inital and final state interactions, and attempt to separate multinucleon absorption from two-nucleon processes.

This work was supported in part by the U.S. Department of Energy, the National Science Foundation and the Robert A. Welch Foundation.

APPENDIX

1. Pion inelastic scattering

In addition to the two- or more-proton data, many events were detected which included a pion and other particles, primarily low-energy charged particles or neutrals. The nonabsorption cross sections and their contribution to the two-proton cross sections are discussed in this section.

The trigger condition for this experiment required that at least two detectors were hit, and so a measure of the

elastic cross section was not obtained. The remaining events which contained a detected pion in the final state are all due to inelastic scattering, charge exchange, and absorption.

Listed in Table IV are the observed cross sections measured in this experiment for final states containing one pion. The cross sections labeled σ_π are for events consisting of only one pion and any number of other particle types. Those labeled as $\sigma_{\pi p}$ are for events consisting of only one pion, one proton, and any number of other particle types. Both of these pion inelastic cross sections are primarily due to quasifree scattering. The total inelastic cross sections for π and πp events can be estimated from the measured pion angular distributions by correcting the observed cross section for the missing solid angle due to the knocked-out particle not being detected. In the $(\pi, \pi' p)$ measurements [34] on C, Fe, and Bi by Piasetzky *et al.* at an incident energy of 245 MeV, the outgoing proton angular distributions were measured and then fitted with narrow and broad Gaussian shapes at various pion angles. The fitted Gaussians were integrated over all space to give the differential $(\pi, \pi' p)$ cross sections $(d^p\sigma/d\Omega_\pi)$ which are listed in Table V at the pion angle nearest to those measured in this experiment.

In principle, the pion angular distributions for πp events measured in this experiment could be corrected for missing solid angle using measurements similar to those made by Ref. [34]. In that work, narrow and broad Gaussians were used to determine a correction factor for the missing proton solid angle at each pion angle. The threshold for detected proton energy was 30 MeV in Ref. [34] which is similar to the threshold for this experiment. Unfortunately, the calculation of the correction factor is complicated by the fact that in Ref. [34] only the amplitude and width parameters for the narrow Gaussian are listed. The widths and amplitudes of the broad Gaussian were not listed, and there is only a statement that the widths of the broad Gaussian are 2–3 times the widths of the narrow Gaussian. For our purposes, the width of the broad Gaussian was assumed to be 3 times the width of the narrow Gaussian. The amplitude of the broad Gaussian was determined by integrating the narrow and broad Gaussians and changing the amplitude of the broad Gaussian until the differential cross section listed in Ref. [34] were obtained. From these parameters for the narrow and broad Gaussians correction factors for the missing proton solid angle were calculated for the measurements at each pion angle and used to correct the measured pion angular distribution. As an indication of the reasonableness of the assumption concerning the width of the broad Gaussian, correction factors were found to be only about 5% different when the width of the broad Gaussian was assumed to be only twice the width of the narrow Gaussian and a different amplitude for the broad Gaussian was determined.

The differential cross sections for $(\pi, \pi' p)$ reactions, labeled as $d\sigma/d\Omega_\pi$ measured in this experiment at 250 MeV are listed in Table V and, given the uncertainties in making these estimates, are seen to be in reasonable agreement with the previous experiment. The same correction factor used for the πp events was used to correct the angular distributions of the π events and the angular

TABLE IV. Pion inelastic cross sections measured in this experiment. In the columns labeled $\sigma_\pi/\sigma_\pi^{\rm est}$, $\sigma_{\pi p}/\sigma_{\pi p}^{\rm est}$, and $\sigma_{\pi 2p}/\sigma_{\pi 2p}^{\rm est}$, the number before the slash is the observed cross section containing an observed π in coincidence with any other particle, one proton, and two protons, respectively. The number after the slash is the estimated total cross section for that final state. If there is no slash, then estimated cross sections were not determined and only the observed cross section is listed. See the discussion in the Appendix for a description of how the correction factors were determined. Previous data, denoted by superscript p, for the total reaction (σ_r^p) [1], total $(\sigma_{\rm total}^p)$ [33], and total inelastic $(\sigma_{\rm inel}^p)$ [1] cross sections are inferred from the systematics of Refs. [1] and [33] for pion energies of 250 and 300 MeV. Previous σ_r^p and $\sigma_{\rm total}^p$ data for ^{12}C at 400 and 500 MeV are from Ref. [23].

T_π (MeV)	Nucleus	$\sigma_{\geq 2h}$ (mb)	σ_r^p (mb)	$\sigma_{\rm total}^p$ (mb)	$\sigma_\pi/\sigma_\pi^{\rm est}$ (mb)	$\sigma_{\rm inel}^p$ (mb)	$\sigma_{\pi p}/\sigma_{\pi p}^{\rm est}$ (mb)	$\sigma_{\pi 2p}/\sigma_{\pi 2p}^{\rm est}$ (mb)
250	^{12}C	180	360	550	55/230	220	25/100	1.9/25
250	^{58}Ni	570	940	1600	130/590	430	54/220	4.5/58
250	^{90}Zr	650	1300	2200	140/600	680	48/190	3.7/48
250	^{118}Sn	910	1500	2600	170/770	820	59/260	4.3/56
250	^{208}Pb	1100	2200	3800	200/870	1100	62/260	3.9/51
300	^{12}C	180	300	445	62/250	200	26/110	2.8/36
300	^{58}Ni	650	810	1400	160/770	390	68/300	8.8/110
300	^{90}Zr	710	1100	1900	150/690	580	60/250	6.8/88
300	^{118}Sn	820	1300	2400	170/810	700	63/289	7.2/94
300	^{208}Pb	1200	1900	3500	230/1000	1000	79/325	7.5/98
400	^{12}C	140	230	380	49		22	3.8/49
400	^{118}Sn	860			180		70	13/170
400	^{208}Pb	1100			210		75	12/160
500	^{12}C	160	220	320	68		25	5.3/69
500	^{58}Ni	720			220		82	20/260
500	^{90}Zr	830			220		77	19/250
500	^{118}Sn	940			250		83	20/260
500	^{208}Pb	1600			360		120	25/325

TABLE V. The $(\pi, \pi' p)$ differential cross sections $(d\sigma/d\Omega_\pi)$ as a function of laboratory scattering angle θ_π obtained in this experiment by integrating over the outgoing proton angular distribution for ^{12}C, ^{58}Ni, and ^{208}Pb nuclei at $T_\pi = 250$ MeV. For comparison are previous measurements, denoted $(d^p\sigma/d\Omega_\pi)$, by Ref. [34] measured on natural C, Fe, and Bi at $T_\pi = 245$ MeV at approximately the same scattering angles.

θ_π (deg)	^{12}C $d\sigma/d\Omega_\pi$ (mb/sr)	C $d^p\sigma/d\Omega_\pi$ (mb/sr)	^{58}Ni $d\sigma/d\Omega_\pi$ (mb/sr)	Fe $d^p\sigma/d\Omega_\pi$ (mb/sr)	^{208}Pb $d\sigma/d\Omega_\pi$ (mb/sr)	Bi $d^p\sigma/d\Omega_\pi$ (mb/sr)
63	6.6	6.4±0.8	11.4	10.8±1.3	11.5	12.5±1.5
79	7.0	6.1±0.7	13.5	12.8±1.5	14.6	15.9±1.9
102	6.9	7.7±0.9	16.1	14.3±1.7	19.6	19.1±2.3
116	7.8	8.7±1.0	20.1	15.0±1.8	23.9	37.2±4.5
142	10.1	9.5±1.1	29.8	17.6±2.1	39.5	25.6±3.1

distributions for the data at $T_\pi = 300$ MeV.

The corrected pion angular distributions for (π, π') and $(\pi, \pi p)$ events were then parametrized with a Legendre polynominal series; only the terms up to $P_2(\cos\theta)$ were necessary to provide a satisfactory description of the distributions. Using this parametrization, the total cross sections were calculated. The total cross sections for pion events $\sigma_\pi^{\rm est}$ are given in Table IV, with an additional correction included for pion knockout of neutrons, expected to be about 1/9 of the proton knockout cross section. The pion inelastic cross sections of Ref. [1] are listed in Table IV. The reasonable agreement with the values of this experiment and the previous measurements give added support to the validity of the corrections applied to the measurements here.

The observed $(\pi, \pi 2p)$ cross sections (i.e., events with only one pion, two protons, and any amount of other particle types) are listed in Table IV. To estimate the correction factor for the observed $(\pi, \pi 2p)$ cross sections due to missing solid angle and detection threshold, an intranuclear cascade (INC) calculation [35] was performed. The nucleus simulated at each incident pion energy of this experiment was ^{12}C. Using the results of this simulation, a correction factor of around 13 for all incident pion energies was found. This correction factor was then used to estimate the total $(\pi, \pi 2p)$ cross section $\sigma_{\pi 2p}^{\rm est}$ listed in Table IV.

Ingram *et al.* [36], in the report of their measurements of ^{16}O pion inelastic quasifree scattering at $T_\pi = 240$ MeV, concluded that 1/4 of the total inelastic cross section involved multistep scattering, and that the multistep processes had an isotropic angular distribution. Using this assumption and the inelastic cross sections from Ref. [1] (listed in Table IV), the total $(\pi, \pi 2p)$ cross sections for C, Ni, and Pb at 250 MeV would be 55, 110, and 280 mb. Using this assumption and the observed cross sections modified by the INC correction factor, the estimated total $\pi 2p$ cross sections would be 25, 58, and 51 mb for C, Ni, and Pb. The discrepancy between the two measurements is a factor of two for C and Ni and a factor of 5 for Pb. The discrepancy might be attributable to the corrections assumed here for the detector threshold for protons in Ref. [1], or validity of the cascade code correction for final state interactions.

While the estimated total $(\pi, \pi 2p)$ cross sections from this experiment are lower than those estimated from previous measurements, we do not believe that the observed $(\pi, \pi 2p)$ cross sections are equally low. A direct comparison of the differential $(\pi, \pi' p)$ cross sections $d\sigma/d\Omega_\pi$ from this experiment to those of Ref. [34] reveal differences much less than a factor of 2. The same is true for the comparison between the $\sigma_\pi^{\rm est}$ for this experiment and the values from Ref. [1]. The corrections to the observed σ_π and $d\sigma/d\Omega_\pi$ are relatively small when compared to the corrections needed for $\sigma_{\pi 2p}$, and so the estimated σ_π and $d\sigma/d\Omega_\pi$ cross sections should be more reliable.

Such comparisons between $\sigma_\pi^{\rm est}$ and $d\sigma/d\Omega_\pi$ obtained here and previous data indicate that our measurements of observed cross sections which involve a pion are reliable enough to use the observed $(\pi, \pi 2p)$ cross sections to estimate the contribution of inelastic pion scattering to the observed $(\pi, 2p)$ cross sections. While there are significant uncertainties in the estimate of this nonabsorption contribution to the $(\pi, 2p)$ cross sections, we note that the observed $(\pi, \pi 2p)$ cross section is generally only about 10% of the observed $(\pi, 2p)$ cross section. The pion distribution in the $(\pi, \pi 2p)$ events is roughly isotropic, which would indicate that the cross section for pion inelastic scattering events in which two protons are observed and the pion is missed is approximately proportional to the missing solid angle, i.e., about 23% of the observed $(\pi, \pi 2p)$ cross section. This would mean that, in general, only about 2% of the observed $(\pi, 2p)$ cross section is caused by pion inelastic scattering events in which the pion was not detected. We can make a very conservative estimate of the contribution of the uncertainty in this value to the uncertainty in the final absorption cross section estimate by applying the factor of three underestimate of the total $(\pi, \pi 2p)$ cross section to the estimate of the contamination and assuming the uncertainty is equal to that value. After subtraction of this and the CEX contribution from σ_{2p}, this uncertainty translates into a relative uncertainty in $\sigma_{\rm abs}^{\rm est}$ in Table III of less than 10% at pion energies below 300 MeV, about 20% at 400 MeV, and 20% for all nuclei at 500 MeV, except for ^{12}C for which it results in a 30% uncertainty. This is comparable to the uncertainty in the Monte Carlo corrections.

2. Single charge exchange reaction

The π^0 from the (π^+, π^0) charge exchange reaction (CEX) decays immediately (10^{-16} s) into two high-

TABLE VI. Observed cross sections for events with two or more observed neutrals. The column labeled $\sigma_{\pi^0}^{est}$ is the estimated total (π^+,π^0) cross section. In the final column are estimates of the total (π^+,π^0) cross sections from Ref. [1].

T_π (MeV)	Nucleus	$\sigma_{2\nu}$ (mb)	$\sigma_{2\nu p}$ (mb)	$\sigma_{2\nu 2p}$ (mb)	$\sigma_{3\nu}$ (mb)	$\sigma_{1\nu+1\ \text{overflow}}$ (mb)	$\sigma_{\pi^0}^{est}$	$\sigma_{\pi^0}^{p}$ (mb)
250	^{12}C	22	8.7	0.97	3.1	0.45	46	47±23
250	^{58}Ni	53	19	1.9	7.2	0.86	110	95±50
250	^{90}Zr	64	20	1.7	10	1.2	140	170±85
250	^{118}Sn	88	29	2.2	13	1.3	190	
250	^{208}Pb	102	31	1.9	15	1.7	220	276±140
300	^{12}C	23	9.6	1.4	4.3	0.87	55	45±22
300	^{58}Ni	59	23	3.0	8.8	2.2	140	98±50
300	^{90}Zr	67	24	3.0	10	2.3	160	154±80
300	^{118}Sn	75	27	3.3	9.6	2.6	170	
300	^{208}Pb	110	38	3.4	18	3.5	260	304±150
400	^{12}C	19	9.8	1.9	4.2	1.6	59	
400	^{118}Sn	78	34	5.5	14	4.5	230	
400	^{208}Pb	98	39	5.5	18	6.8	290	
500	^{12}C	20	10	2.4	6.0	3.2	91	
500	^{58}Ni	66	33	7.7	16	9.4	290	
500	^{90}Zr	74	34	8.1	17	9.8	320	
500	^{118}Sn	75	37	8.2	14	9.3	320	
500	^{208}Pb	130	55	10	30	17	550	

energy photons. Because of the high detection efficiency for photons, if both of these enter detectors in the BGO array the probability is nearly 100% that they will be observed as two neutral hits. Indeed, the event may result in more than two neutral hits, since a shower close to a boundary of two detectors can give a signal in both. Because of the much lower detection efficiency for neutrons, we will first assume that all events with two or more neutrals are due to CEX. This is supported by the phase space calculations in Sec. IV. We then observe the fraction of those events which also contain two or more protons. Next we model the CEX scattering and estimate the probability that only one or neither photon is observed and make appropriate corrections to the observed two proton cross sections.

The observed cross sections for 2ν, $2\nu p$, $2\nu 2p$, and 3ν (where ν indicates a neutral and p an identified proton) events are listed in Table VI. The 3ν events appear to be mainly π^0 decays in which the shower from one of the photons spread into two adjacent detectors. Also given in Table VI are the observed cross section for $1\nu+1$ overflow events. It appears that most overflows (in which the deposited energy is greater than about 220 MeV) are neutrals, and so the $1\nu+1$ *overflow* events should probably be included as part of the 2ν cross section.

To estimate the total (π^+,π^0) cross section, a correction must be made for the missing solid angle of the BGO ball. This correction was estimated by a Monte Carlo calculation in which the angular distribution and energy of the π^0 was assumed to be the same as in the free case, except that scatters in which the recoil proton had an energy of less than 15 MeV were rejected to simulate the effects of Pauli blocking. The π^0 decay was assumed isotropic in its center of mass and the fraction in which zero, one, or two photons hit the BGO ball was then found. The fractions are given in Table VII for different incident pion energies. There is a strong energy dependence as both the cross sections and the direction of the decay photons become increasingly forward peaked at higher incident pion energies.

The observed cross sections for events with 2ν, 3ν, and $1\nu+1$ *overflow* were added together and multiplied by a correction factor to give the total (π^+,π^0) cross section listed in Table VI. The measurements reported here represent the first measurements of the total (π^+,π^0) cross sections at these incident pion energies on these targets. However, there estimates have been made by Ref. [1] for incident pion energies of 245 and 315 MeV for a variety of targets. A comparison to these estimates is shown in Table VI. Our values are within one standard deviation of the estimates of Ref. [1].

From Table VII we see that the ratio of events with two observed photons to those with either one or both photons undetected is 1:1, 1:1, 1:1.4, and 1:2 for incident pion energy of 250, 300, 400, and 500 MeV, respectively. For ^{12}C the observed $2p2\nu$ cross sections are 4%, 6%, 11%, and 13% of the observed $2p$ cross sections at these incident energies, respectively. Thus the CEX contaminations of the ^{12}C observed $2p$ cross sections are 4%, 6%,

TABLE VII. Calculated fraction of the total (π^+,π^0) cross section observed with two photons (2γ), one photon (1γ), and no photons (no γ) detected in the BGO ball. The calculations are described in the Appendix.

T_π	2γ	1γ	no γ
250	0.55	0.39	0.06
300	0.51	0.41	0.08
400	0.42	0.44	0.14
500	0.32	0.49	0.19

15%, and 26%, respectively. For the heavier nuclei, the observed cross sections for $2p2\nu$ vary from 2% to 6% of the observed $2p$ cross sections as the incident pion energy increases from 250 to 500 MeV, giving a CEX contaminations of the observed $2p$ cross section of less than 12%. The relative uncertainty of the CEX contamination to the $2p$ cross section was taken conservatively as 30% for pion energies of 250 and 300 MeV and 50% for pion energies of 400 and 500 MeV. This contributes an uncertainty of less than 10% to the estimated $2p$ absorption cross section in Table III for 250 MeV, about 20% for 300 MeV, and about 30% for 400 and 500 MeV. As with the inelastic contribution discussed above, this is comparable to the uncertainty of the Monte Carlo correction.

[1] D. Ashery, I. Navon, G. Azuelos, H. K. Walter, H. J. Pfeiffer, and F. W. Schlepütz, Phys. Rev. C **23**, 2173 (1981).

[2] D. Ashery and J. P. Schiffer, Annu. Rev. Nucl. Part. Sci. **36**, 207 (1986).

[3] G. Backenstoss, M. Iżycki, P. Salvisberg, M. Steinacher, P. Weber, H. J. Weyer, S. Cierjacks, S. Ljungfelt, H. Ullrich, M. Furić, and T. Petković, Phys. Rev. Lett. **55**, 2782 (1985).

[4] K. A. Aniol, A. Altman, R. R. Johnson, H. W. Roser, R. Tacik, U. Wienands, D. Ashery, J. Alster, M. A. Moinester, E. Piasetzky, D. R. Gill, and J. Vincent, Phys. Rev. C **33**, 1714 (1986).

[5] G. Backenstoss, M. Iżycki, P. Salvisberg, M. Steinacher, P. Weber, H. J. Weyer, S. Cierjacks, B. Rzehorz, H. Ullrich, M. Furić, T. Petković, and N. Simicevic, Phys. Rev. Lett. **59**, 767 (1987).

[6] G. Backenstoss, D. Brodbeck, M. Iżycki, P. Salvisberg, M. Steinacher, P. Weber, H. J. Weyer, A. Hoffart, B. Rzehorz, H. Ullrich, D. Bosnar, M. Furić, and T. Petković, Phys. Rev. Lett. **61**, 923 (1988).

[7] M. Steinacher, G. Backenstoss, M. Izycki, P. Salvisberg, P. Weber, H. J. Weyer, A. Hoffart, B. Rzehorz, H. Ullrich, M. Dzemidzić, M. Furić, and T. Petkovic, Nucl. Phys. **A517**, 413 (1990).

[8] S. Mukhopadhyay, S. Levenson, R. E. Segel, G. Garino, D. F. Geesaman, J. P. Schiffer, G. Stephans, B. Zeidman, E. Ungricht, H. Jackson, R. Kowalczyk, D. Ashery, E. Piasetsky, M. Moinester, I. Navon, L. C. Smith, R. C. Minehart, G. S. Das, R. R. Whitney, R. Mckeown, B. Anderson, R. Madey, and J. Watson, Phys. Rev. C **43**, 957 (1991).

[9] P. Weber, J. McAlister, R. Olszewski, A. Feltham, M. Hanna, R. R. Johnson, M. Pavan, C. Ponting, F. M. Rozon, M. Sevior, V. Sossi, D. Vetterli, D. Humphrey, G. J. Lolos, Z. Papandreou, R. Tacik, D. Ottewell, G. Sheffer, G. R. Smith, Y. Mardor, and S. May-Tal, Phys. Rev. C **43**, 1553 (1991).

[10] P. Weber, G. Backenstoss, M. Izycki, P. Salvisberg, R. J. Powers, M. Steinacher, S. Cierjacks, A. Hoffart, B. Rzehorz, H. Ullrich, H. J. Weyer, N. Bosnar, M. Furić, T. Petkovic, and N. Simicevic, Nucl. Phys. **A534**, 541 (1991).

[11] F. Adimi, H. Breuer, B. S. Flanders, M. A. Khandaker, M. G. Khayat, P. G. Roos, D. Zhang, Th. S. Bauer, J. Konijn, C. T. A. M. de Laat, G. S. Kyle, S. Mukhopadhyay, M. Wang, and R. Tacik, Phys. Rev. C **45**, 2589, (1992).

[12] L. C. Smith, R. C. Minehart, D. Ashery, E. Piasetsky, M. Moinester, I. Navon, D. F. Geesaman, J. P. Schiffer, G. Stephens, B. Zeidman, S. Levenson, S. Mukhopadhyay, R. E. Segel, B. Anderson, R. Madey, J. Watson, and R. R. Whitney, Phys. Rev. C **40**, 1347 (1989).

[13] E. Oset, Y. Futami, and H. Toki, Nucl. Phys. **A448**, 597 (1986).

[14] K. Masutani and K. Yazaki, Nucl. Phys. **A407**, 309 (1983).

[15] G. E. Brown, H. Toki, W. Weise, and A. Wirzba, Phys. Lett. **118B**, 39 (1982).

[16] R. Tacik, E. T. Boschitz, W. Gyles, W. List, and C. R. Otterman, Phys. Rev. C **32**, 1335 (1985).

[17] R. Tacik, E. T. Boschitz, W. Gyles, W. List, C. R. Otterman, M. Wessler, U. Wiedner, and R. R. Johnson, Phys. Rev. C **40**, 256 (1989).

[18] R. D. Ransome, V. R. Cupps, S. Dawson, R. W. Fergerson, A. Green, C. L. Morris, J. A. McGill, J. R. Comfort, B. G. Ritchie, J. Tinsley, J. D. Zumbro, R. A. Loveman, P. C. Gugelot, D. L. Watson, and C. Fred Moore, Phys. Rev. Lett. **64**, 372 (1990); Phys. Rev. C **42**, 1500 (1990).

[19] R. D. Ransome, in *Pion-Nucleus Physics: Future Directions and New Facilities at LAMPF*, Proceedings of the Los Alamos Conference on Pion-Nucleus Physics, AIP Conf. Proc. No. 163, edited by R. J. Peterson and D. D. Strottman (AIP, New York, 1988), p. 270.

[20] R. L. Craun and D. L. Smith, Nucl. Instrum. Methods **80**, 239 (1970).

[21] W. O. Lock and D. F. Measday, *Intermediate Energy Nuclear Physics* (Methuen, London, 1970), p. 256.

[22] M. J. Borkowsky, V. G. Gaditsky, G. E. Gavrilov, V. A. Gordeev, and Yu. S. Grigir'ev, J. Phys. G **11**, 69 (1985).

[23] W. O. Lock and D. F. Measday, *Intermediate Energy Nuclear Physics* (Methuen, London, 1970), p. 281.

[24] F. James, CERN Computer Program Library W515, 1975.

[25] B. G. Ritchie, Phys. Rev. C **44**, 533 (1991).

[26] R. D. Ransome, C. L. Morris, V. R. Cupps, R. W. Fergerson, J. A. McGill, D. L. Watson, J. D. Zumbro, B. G. Ritchie, J. R. Comfort, J. R. Tinsley, R. A. Loveman, S. Dawson, A. Green, P. C. Gugelot, and C. Fred Moore, Phys. Rev. C **45**, 509 (1992).

[27] A. Altman, D. Ashery, E. Piasetzky, J. Lichtenstadt, A. I. Yavin, W. Bertl, L. Felawka, H. K. Walter, R. J. Powers, R. G. Winter, and J. v. d. Pluym, Phys. Rev. C **34**, 1757 (1986).

[28] S. D. Hyman, D. J. Mack, H. Breuer, N. S. Chant, F. Khazaie, B. G. Ritchie, P. G. Roos, J. D. Silk, P.-A. Amaudruz, Th. S. Bauer, C. H. Q. Ingram, G. S. Kyle, D. Renker, R. A. Schumacher, U. Sennhauser, and W. J. Burger, Phys. Rev. C **41**, R409 (1990).

[29] W. J. Burger, E. Beise, S. Gilad, R. P. Redwine, P. G. Roos, N. S. Chant, H. Breuer, G. Ciangaru, J. D. Silk, G. S. Blanpied, B. M. Preedom, B. G. Ritchie, M. Blecher, K. Gotow, D. M. Lee, and H. Ziock, Phys. Rev. Lett. **57**, 58 (1986); Phys. Rev. C **41**, 2215 (1990).

[30] W. Brückner, H. Döckner, H. Döbbeling, P. C. Gugelot, F. Güttner, H. Kneis, S. Majewski, M. Nomachi, S. Paul,

B. Povh, R. D. Ransome, T.-A. Shibata, M. Treichel, Th. Walcher, P. Amaudruz, Th. Bauer, J. Domingo, R. Frey, Q. Ingram, H. Jantzen, G. Kyle, D. Renker, and R. A. Schumacher, Nucl. Phys. **469A**, 617 (1987).

[31] M. B. Golubeva, E. S. Golubeva, F. F. Guber, T. L. Karavicheva, Yu. G. Kudenko, A. B. Kurepin, A. I. Reshetin, and N. S. Topilskaya, Phys. Lett. B **221**, 238 (1989).

[32] R. D. McKeown, S. J. Sanders, J. P. Schiffer, H. E. Jackson, M. Paul, J. R. Specht, E. J. Stephenson, R. P. Redwine, and R. E. Segel, Phys. Rev. C **24**, 221 (1981).

[33] A. S. Carroll, I-H. Chiang, C. B. Dover, T. F. Kycia, K. K. Li, P. O. Mazur, D. N. Michael, P. M. Mockett, D. C. Rahm, and R. Rubinstein, Phys. Rev. C **14**, 635 (1976).

[34] E. Piasetzky, D. Ashery, A. Altman, A. I. Yavin, F. W. Schepütz, R. J. Powers, W. Bertl, L. Felawka, H. K. Walter, R. G. Winter, and J. v. d. Pluym, Phys. Rev. C **25**, 2687 (1982).

[35] W. R. Gibbs and W. B. Kaufmann, in *Pion-Nucleus Physics: Future Directions and New Facilities at LAMPF*, Proceedings of the Los Alamos Conference on Pion-Nucleus Physics, AIP Conf. Proc. No. 163, edited by R. J. Peterson and D. D. Strottman (AIP, New York, 1988), p. 279; W. R. Gibbs (private communication).

[36] C. H. Q. Ingram, P. A. M. Gram, J. Jansen, R. E. Mischke, J. Zichy, J. Bolger, E. T. Boschitz, G. Pröbstle, and J. Arvieux, Phys. Rev. C **27**, 1578 (1983).